Available online at www.sciencedirect.com

ScienceDirect

Ceramics International 40 (2014) 4607–4616

CERAMICS INTERNATIONAL

www.elsevier.com/locate/ceramint

Improved visible light photocatalytic activity of MWCNT/BiOBr composite synthesized via a reactable ionic liquid

Jiexiang Xia[a], Jun Di[a], Sheng Yin[a], Huaming Li[a,*], Li Xu[b], Yuanguo Xu[a], Chunyan Zhang[a], Huoming Shu[c]

[a]School of Chemistry and Chemical Engineering, Jiangsu University, 301 Xuefu Road, Zhenjiang 212013, PR China
[b]School of Material Science and Engineering, Jiangsu University, Zhenjiang 212013, PR China
[c]Department of Chemistry, Hainan Normal University, Haikou 571158, PR China

Received 15 August 2013; received in revised form 31 August 2013; accepted 1 September 2013
Available online 7 September 2013

Abstract

Novel flower-like MWCNT/BiOBr composite photocatalysts have been prepared through a one-pot EG-assisted solvothermal process in the presence of reactable ionic liquid 1-hexadecyl-3-methylimidazolium bromide ([C_{16}mim]Br). The structures, morphology and photocatalytic properties of as-prepared samples were characterized by X-ray diffraction (XRD), scanning electron microscopy (SEM), transmission electron microscopy (TEM), energy-dispersive X-ray spectroscopy (EDS), Fourier transform spectrophotometer(FT-IR), diffuse reflectance spectroscopy (DRS), photoluminescence (PL) spectroscopy, photocurrent and electrochemical impedance spectroscopy (EIS). During the reactive process, ionic liquid [C_{16}mim]Br acted as solvents, reactants, templates and MWCNT dispersing agents. The MWCNT/BiOBr composite photocatalysts exhibited a conspicuous improved photocatalytic performance for rhodamine B (RhB) degradation. The optimal MWCNT content for the photocatalytic activity was determined. The DRS analysis showed that the prepared MWCNT/BiOBr composites exhibited strong absorption ability with the increase of doped MWCNT amount. The results of PL, EIS and photocurrent analysis indicated that MWCNT could disperse and combine with BiOBr microspheres on its surface, which facilitated electron–hole separation, and contributed to improve the photocatalytic activity. The radicals trap experiments demonstrated that hole was the main reactive species during the degrading process of RhB. A possible mechanism for the enhanced photocatalytic activity of MWCNT/BiOBr was also proposed.

Keywords: BiOBr; Composite; Ionic liquid; MWCNT; Photocatalytic

1. Introduction

In recent years, much attention has been focused on bismuth-based oxyhalides (BiOX, X=Cl, Br, I). This new type of semiconductor materials has potential photocatalysis application [1–3] because of its unique and excellent electrical and optical properties [4,5]. Besides, it can also be applied in ionic conduction, ferroelectric materials and pigments [6,7].

Among these BiOX catalysts, BiOBr is of great research interest because it is an active and stable visible-light photocatalyst and it has advantageous performance under visible-light irradiations [8]. BiOBr is an important V–VII ternary compound which crystallizes in the tetragonal matlockite structure. The layer structure characterized by [Bi_2O_2] slabs interleaved by double slabs of halogen atoms [9].

At present, BiOBr with different structures and morphologies prepared by using different synthetic methods is still among hot research [1,8,10–14]. However, its photocatalytic activity has been limited by the high recombination of its photogenerated electron–hole pairs. In order to improve their performance, different modifications of BiOBr matrix material have been used. These modifications include coupling BiOBr with g-C_3N_4 [15], Graphene [16], $Bi(OH)_3$ [17], BiOI [18], BiOCl [19], $ZnFe_2O_4$ [20], AgBr [21] or doping metals like Ag [22], Fe [23]. The results indicate that coupling is benefit to the enhancement of the photocatalyst activity. Therefore, it can be expected that the formation of composite materials could further improve the photocatalytic activity of BiOBr.

In recent years, the carbon nanotubes (CNT) have received much more interests due to its hollow geometrical structures

*Corresponding author. Tel./fax: +86 511 88791108.
E-mail addresses: xjx@ujs.edu.cn (J. Xia), lhm@ujs.edu.cn (H. Li).

0272-8842/$ - see front matter © 2013 Elsevier Ltd and Techna Group S.r.l. All rights reserved.
http://dx.doi.org/10.1016/j.ceramint.2013.09.001

and excellent electron conductivity. It is possible to accelerate the transfer of electrons between the nanostructure interfaces [24–26]. The carbon nanotubes coupled with semiconductor composites have been synthesized, such as MWCNT/TiO_2 [27–29], BiOI-MWCNT [30], MWNTs/g-C_3N_4 [31], MWC NTs/CdS [32], MWCNT/ZnS [33], and the results inferred that the introduction of carbon nanotubes could improve the photocatalytic degradation activity of the semiconductor photocatalysts. Considering carbon nanotubes have the large specific surface areas and the excellent charge transfer properties, it motivates us to design MWCNT/BiOBr composites that are expected to be a promising candidate of efficient photocatalysts.

Ionic liquids (ILs) have aroused increasing interest due to their high fluidity, low melting temperature, thermal stability, extended liquid-state temperature range, high ionic conductivity, ability to dissolve a variety of materials and nearly zero vapor pressures. Due to the advantages of ILs, many kinds of materials have been successfully synthesized in ILs, such as Au nanosheets [34], Pd Nanoparticles [35], high-quality TiO_2 nanocrystals [36], CuS nest-like hollow spheres [37], nanoflower Y_2O_3 [38], Bi_2S_3, Sb_2S_3 nanorods [39], CuCl nanoplatelets [40], ZnO nanoparticles and nanowires [41] and ultrathin $SmVO_4$ nanosheets [42]. The researches show that ILs acted as good dispersing agents, solvents and templates, contributing to the synthesis of functional materials. It is also well studied that the ionic liquids could combined with CNT due to the possible specific interaction between the imidazolium ion component and the pi-electronic nanotube surface [43,44]. Inspired by this, reactable ionic liquid has been designed and used in the synthesis of MWCNT/BiOBr composites. The potential of ionic liquids in the controlled synthesis of MWCNT/BiOBr composites remains to be explored.

In this work, the novel MWCNT/BiOBr composites have been prepared through a facile one-pot EG-assisted solvothermal process in the presence of reactable ionic liquid [C_{16}mim]Br. During the reactive process, ionic liquid [C_{16}mim]Br acted as solvent, reactant, template and MWCNT dispersing agent at the same time. The obtained composites showed higher photocatalytic activity than pure BiOBr. The effect of MWCNT contents on the photocatalytic degradation efficiency was investigated. The characterization of the samples indicated that MWCNT could disperse and combine well with BiOBr microspheres on its surface, which facilitated electron–hole separation, and may lead to enhance the visible light photocatalytic activity. The radicals trap experiments demonstrated that hole was the main reactive species for the degradation of RhB. A possible mechanism for the enhanced photocatalytic activity of MWCNT/BiOBr was also proposed.

2. Experimental

2.1. Material and sample preparation

All chemicals were analytical grade and used without further purification. The ionic liquid [C_{16}mim]Br (1-hexadecyl-3-methylimidazolium bromide) (99%)was purchased from Shanghai Chengjie Chemical Co. Ltd. The MWCNT (MWCNT-NH_2, purity > 95%) was purchased from Chengdu Organic Chemicals Co. Ltd., Chinese Academy of Sciences.

2.2. Fabrication of MWCNT/BiOBr composite photocatalysts

In a typical procedure, 5 mg multi-walled carbon nanotubes (MWCNT) were dispersed into 200 mL of ethylene glycol with ultrasonic treatment for 30 min and stirred for 3 days to make MWCNT totally dispersed. 1 mmol of ionic liquid [C_{16}mim]Br was dissolved into a certain amount of MW CNT/EG solution with magnetic stirring for 30 min to make the ionic liquid interact with MWCNT and then stoichiometric amounts of $Bi(NO_3)_3 \cdot 5H_2O$ were dissolved. The mixture was stirred for 30 min and was transferred into 25 mL Teflon-lined autoclave up to 80% of the total volume. The autoclave was then heated at 140 °C for 24 h and cooled down to room temperature. The final product was collected by centrifugation and washed with deionized water and ethanol for three times, and then dried under vacuum at 50 °C for 24 h before photocatalytic reaction and further characterizations. The weight contents of MWCNT in the composite photocatalysts were 0, 0.01%, 0.05%, 0.1%, 1%, respectively.

2.3. Characterization

X-ray powder diffraction (XRD) analysis was carried out on a Bruker D8 diffractometer with high-intensity Cu-Kα (λ=1.54 Å). X-ray photoemission spectroscopy (XPS) was recorded on a VG MultiLab 2000 system with a monochromatic Mg Kα source operated at 20 kV. The field-emission scanning electron microscopy (FE-SEM) measurements were carried out with a field-emission scanning electron microscope (JEOL JWSM-7001F) equipped with an energy-dispersive X-ray spectroscope (EDS) operated at an acceleration voltage of 10 kV. Transmission electron microscopy (TEM) micrographs were taken with a JEOL-JEM-2010 (JEOL, Japan) operating at 200 kV. UV–vis diffuse reflectance spectroscopy was recorded on an UV-2450 spectrophotometer (Shimadzu Corporation, Japan) using $BaSO_4$ as the reference. The structural information for samples was measured by Fourier transform spectrophotometer (FT-IR, Avatar 470, Thermo Nicolet) using the standard KBr disk method. The PL spectra of the photocatalysts were detected using a Varian Cary Eclipse spectrometer. Photocurrent and electrochemical impedance spectroscopy (EIS) were performed on an electrochemical workstation (CHI 660B Chenhua Instrument Company, Shanghai, China).

2.4. Photocurrent and EIS measurements

The photocurrent and EIS measurements were conducted by using an electrochemical analyzer (CHI660B, Chen Hua Instruments, Shanghai, China) with a standard three-electrode configuration. A 500 W xenon lamp was used as photosource. The working electrodes were ITO glass (0.5 × 1 cm^2) coated with as-prepared samples (0.1 mg), the counter electrode was

a platinum wire, and the reference electrode was a saturated Ag/AgCl electrode. The electrolyte solution of photocurrent was phosphate buffered saline (PBS) (0.1 mol L^{-1}, pH = 7.0). The EIS were performed in a 0.1 M KCl solution containing 5 mM $Fe(CN)_6^{3-}$/$Fe(CN)_6^{4-}$. Sunless conditions were ensured when experiments were carried out.

2.5. Photocatalytic activity measurement

Photocatalytic activities of the prepared samples were evaluated by the photocatalytic degradation of RhB under the visible light irradiation. Experiments were carried out in a Pyrex photocatalytic reactor with a 300 W Xe lamp with a UV cutoff filter ($\lambda > 400$ nm) as the visible-light source, and a circulating water system to prevent thermal catalytic effects. Aeration was performed using an air pump to make sure a constant supply of oxygen and to mix the solution with photocatalysts fully during photoreactions. In a typical photocatalytic experiment, 0.01 g of MWCNT/BiOBr powders was dispersed into 100 mL of RhB (10 mg L^{-1}) solutions. Prior to irradiation, the solution was stirred magnetically in the dark for 30 min in order to reach the adsorption equilibrium between the photocatalyst and the RhB. During irradiation, about 3 mL of the suspension was withdrawn periodically from the reactor cell. With the process of the irradiation, the intense red color of the RhB solution gradually faded. The photocatalyst powders and the RhB solution were separated by centrifuge. The RhB concentration was analyzed by a UV–vis spectrophotometer (Shimadzu, UV-2450), the absorbance wavelength is 553 nm.

3. Results and discussion

3.1. XRD analysis

Fig. 1 shows the XRD patterns of the MWCNT/BiOBr composites of varying MWCNT contents. The results showed that the photocatalysts were well crystallized. All the samples had similar diffraction peaks, which were readily indexed to the tetragonal phase of BiOBr (JCPDS card No. 73-2061).

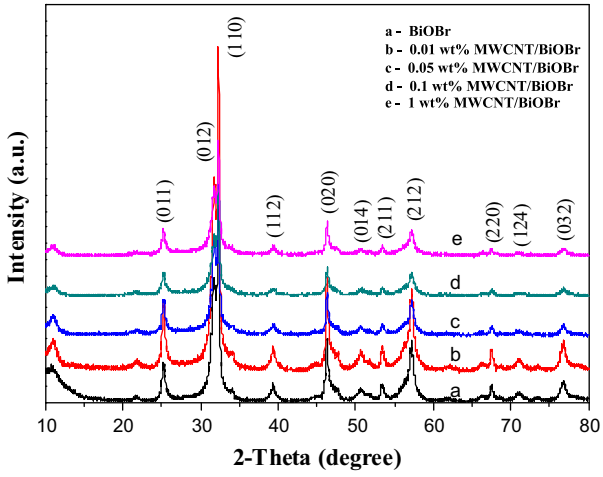

Fig. 1. The XRD pattern of the as-prepared MWCNT/BiOBr composites with different contents of MWCNT.

No diffraction peaks corresponding to MWCNT were observed in MWCNT/BiOBr composites. This was due to the trace amount of loading MWCNT with a low atomic number cannot be resolved by XRD. The result can also be found in the similar system [32]. No other characteristic peaks were found, indicating the high purity of the as-prepared samples. The existence of MWCNT was identified by SEM, TEM and EDS.

3.2. XPS analysis

To investigate the states of the ions, the MWCNT/BiOBr composite was studied by X-ray photoelectron spectroscopy (XPS) (Fig. 2). The XPS analysis showed that the composites were composed of elements of Bi, O, Br, and C. The carbon peak probably came from the MWCNT and the adventitious carbon on the surface of the sample. And, the existence of MWCNTs has been further confirmed in the SEM, TEM and EDS results. The high-resolution spectra of Fig. 2c displayed that the two strong peaks at 159.0 eV and 164.4 eV were assigned to Bi 4f7/2 and Bi 4f5/2, respectively, which was characteristic of Bi^{3+} in the composites. The Br 3d peaks were associated with binding energy of 68. 04 eV (Fig. 2d), which was characteristic of Br^- in the composites. The high-resolution spectra of Fig. 2e showed that the peak at binding energies of 529.7 eV was assigned to O 1s, which was characteristic of oxygen in BiOBr materials. As a result, it can be confirmed that the MWCNT/BiOBr composites have been successfully synthesized.

3.3. FT-IR spectra analysis

The infrared spectrum of MWCNT/BiOBr composites prepared is shown in Fig. 3. The absorption peak around 1630 cm^{-1} corresponded to the bending vibrations of O–H, which was ascribed to the water adsorbed. The absorption band at 510 cm^{-1} was ascribed to the Bi–O stretching mode. No characteristic absorption peak of the ionic liquids was found in the FT-IR spectra, which could lead to the assumption that the ionic liquid can be easily removed from the surface of the material by washing with deionized water and alcohol.

3.4. SEM, TEM and EDS analysis

The SEM images of the 0.05 wt% MWCNT/BiOBr composite have been shown in Fig. 4a. It can be seen that sphere-like MWCNT/BiOBr structures were formed with an average diameter of 1–2 μm. The sphere-like MWCNT/BiOBr composite prepared was self-assembled generated by irregular BiOBr nanosheets. It can be seen clearly from the Fig. 4b,c that a large number of MWCNT attached to the surface of MWCNT/BiOBr microspheres. As can be seen clearly from the high magnification SEM image (Fig. 4d), the MWCNT attached, embedded and interwoven on the surface of BiOBr nanosheets. The sphere-like MWCNT/BiOBr composites were further investigated by TEM, as shown in Fig. 5. The result further confirmed that the composites were spheres-like structures. The detailed structure was also characterized by HRTEM (Fig. 5b). As can be seen, the lattice structure of BiOBr was

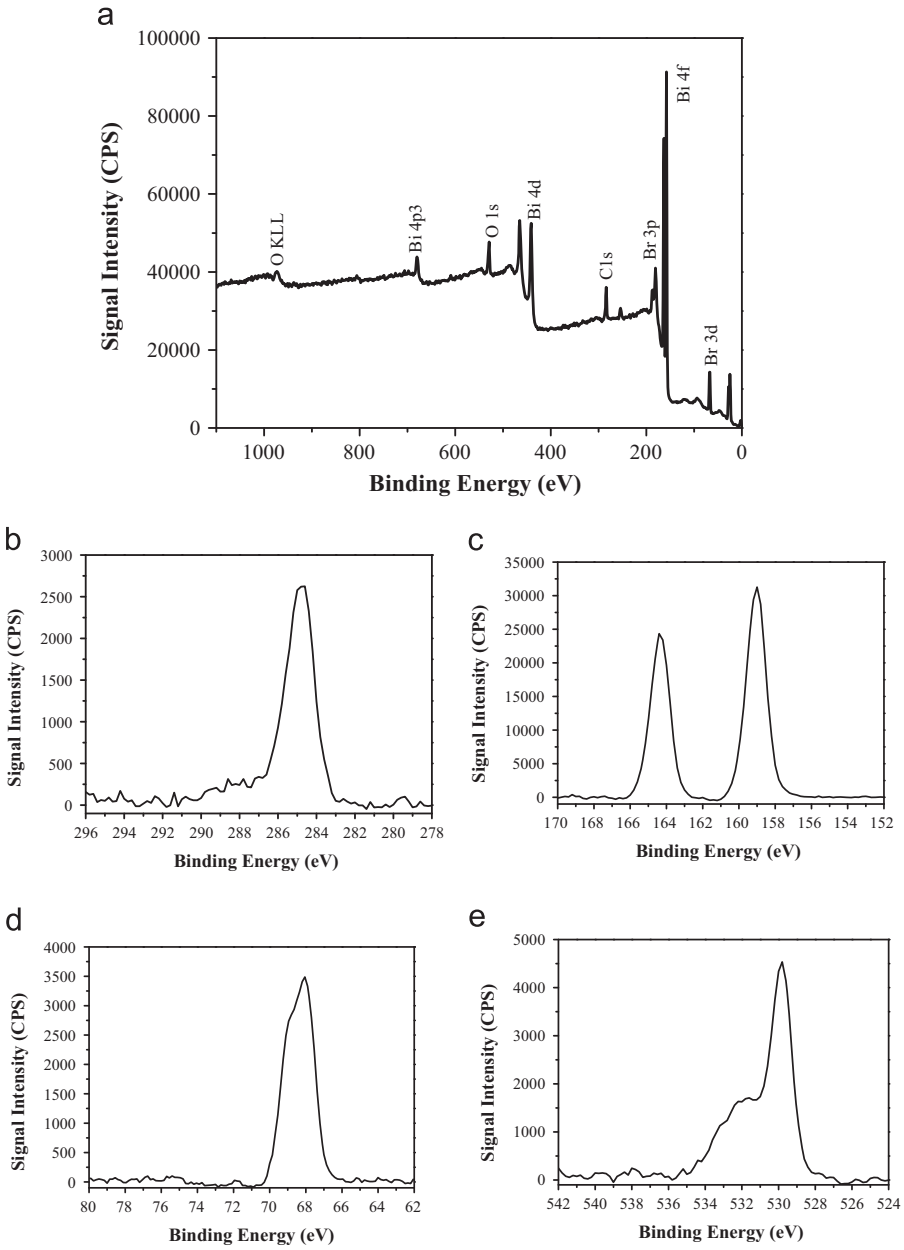

Fig. 2. XPS spectra of the as-prepared 0.05 wt% MWCNT/BiOBr composites. (a) Survey of the sample; (b) C 1s, (c) Bi 4f, (d) Br 3d and(e) O 1s.

orderly. The outer boundary of the MWCNT/BiOBr composites has some MWCNTs which were different from the BiOBr crystal. The clear lattice fringes of the interplane of the BiOBr core was 0.28 nm in the HRTEM image, which was in accordance with the [110] direction of BiOBr crystal. The EDS pattern (Fig. 4e) indicated that the MWCNT/BiOBr composites contained C, O, Bi, and Br element. It proved that the sample prepared was MWCNT/BiOBr composite material. This result consisted with the result of XPS, SEM and TEM analysis.

3.5. Optical absorption properties

In order to investigate the optical properties, the as-prepared MWCNT/BiOBr samples were analysed by UV–vis absorption spectra in the wavelength range of 200–800 nm, and the spectra was given in Fig. 6a. The absorption intensity of the as-prepared samples strengthened with increasing MWCNT content (from 0 wt% to 1.0 wt%), which was in agreement with the color change from white to black. Compared with the pure BiOBr sample, MWCNT/BiOBr samples have apparently red shift, which means it enhanced light absorption. The enhanced light absorption of the MWCNT/BiOBr composites resulted in the generation of more electron–hole pairs under the same visible light irradiation, which subsequently could lead to a higher photocatalytic activity.

The band structure of the photocatalyst was responsible for the difficulty degree of the electronic transitions. A lower band gap was beneficial to the electronic transitions. As can be seen from Fig. 6b, the band gap of pure BiOBr was about 2.8 eV.

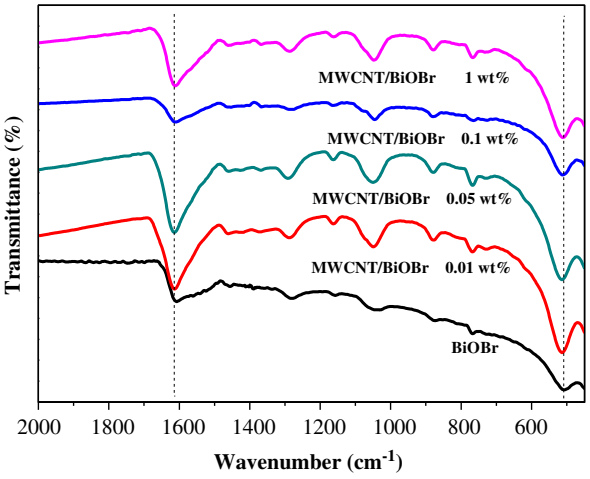

Fig. 3. FT-IR analysis of MWCNT/BiOBr materials with different contents of MWCNT.

With the addition of MWCNT, the band gaps of MWCNT/BiOBr composites were decreased. It can be judged preliminary that MWCNT/BiOBr composites had good response in the visible region and then form more electron–hole pairs. It can be further speculated that the MWCNT/BiOBr composites have enhanced degradation activity of organic pollutants in visible light.

3.6. Photoluminescence spectra analysis

To investigate the effect of the MWCNT, photoluminescence spectra analysis was applied to reveal the migration and recombination processes of photo-generated electron–hole pairs in MWCNT/BiOBr composite samples. Fig. 7 presents the PL spectra for BiOBr and 0.05 wt% MWCNT/BiOBr with an excitation wavelength of 360 nm. After the photocatalyst was irradiated, electron–hole pairs recombination occurred, photons were emitted, those lead to photoluminescence. A weaker intensity of the peak represented a lower recombination probability of photogenerated charge carriers. The intensity of the 0.05 wt% MWCNT/BiOBr composite photocatalyst was much lower than that of pure BiOBr, which indicated that the 0.05 wt% MWCNT/BiOBr composite had a much lower recombination rate of photo-generated charge carriers. This result indicated that the doping of MWCNT reduced the recombination efficiency of electron–hole pairs which was favorable for enhancing photocatalytic activity of BiOBr. It can be inferred that the prepared 0.05 wt% MWCNT/BiOBr composite had a higher photocatalytic activity than pure BiOBr.

3.7. Photocurrent

To understand better about the electron transfer process, the photocurrent of BiOBr and 0.05 wt% MWCNT/BiOBr under visible light was measured as shown in Fig. 8. When the lamp turns on, the photocurrent increased sharply, reaching a stable value. As soon as the lamp turns off, the photocurrent rapidly decreased to initial status. In general, a higher photocurrent would mean the presence of longer living photogenerated carriers and hence a higher photocatalytic activity. It can be seen from the diagram that the current intensity of 0.05 wt% MWCNT/BiOBr was 1.5 times of pure BiOBr. This finding suggested that the introduction of MWCNT could elevate the separation efficiency of electrons and holes, so it could produce longer living photogenerated carriers. Therefore, compared with pure BiOBr,0.05 wt% MWCNT/BiOBr was expected to exhibit an enhanced photocatalytic activity.

3.8. Electrochemical impedance spectroscopy

EIS measurement has been employed to research the charge transfer resistance and the separation efficiency between the photogenerated electrons and holes. It could be seen from Fig. 9 that the arc radius on EIS of 0.05 wt% MWCNT/BiOBr was smaller than that of BiOBr. It indicated that 0.05 wt% MWCNT/BiOBr had lower resistance than that of pure BiOBr, which could accelerate the interfacial charge-transfer process [45]. This result demonstrated that the introduction of MWCNT into BiOBr could elevate the separation and transfer efficiency of photogenerated electron–hole pairs [46], and then contribute to improving photocatalytic activity of BiOBr.

3.9. Photocatalytic performance

RhB was selected as target pollutant to measure the photocatalytic activity under the visible-light irradiation. Fig. 10a shows the time-dependent absorption spectra of RhB solution in the presence of 0.05 wt% MWCNT/BiOBr composite. The intensity of the absorption peak at 553 nm decreased drastically within 75 min. The degradation efficiency reached 97% after 75 min irradiation, which indicated that the 0.05 wt% MWCNT/BiOBr composite exhibited high photocatalytic activity. The peak intensity of the UV–vis absorption related to RhB decreased evidently, and the maximum absorption of the RhB solution shifted from 553 to 500 nm after irradiation for 75 min. In order to study the effect of MWCNT, photocatalytic degradation experiments of MWCNT/BiOBr with different MWCNT contents were carried out using RhB in an aqueous suspension under visible-light irradiation. Fig. 10b shows the degraded effect of pure BiOBr and MWCNT/BiOBr composites with different MWCNT contents. As shown in Fig. 10b, the 0.05 wt% MWCNT/BiOBr composite exhibited the highest photocatalytic activity. Only 31.3% RhB was photodegraded by pure BiOBr after irradiation for 30 min, while the 0.05 wt% MWCNT/BiOBr photodegraded 77.4%. After 75 min irradiation, the degradation efficiency of the 0.05 wt% MWCNT/BiOBr reached 97%. The photocatalytic results indicated that the doping amount of MWCNT had a significant effect on the photocatalytic performance of the MWCNT/BiOBr composite photocatalysts. Contrasting to the MWCNT combined photocatalysisTiO_2/MWCNT [47], MoO_3/MWCNT [48] and ZnO/MWCNT [49], all the results showed that the introduction of MWCNT could improve the photocatalytic ability of the composites, and MWCNT/BiOBr

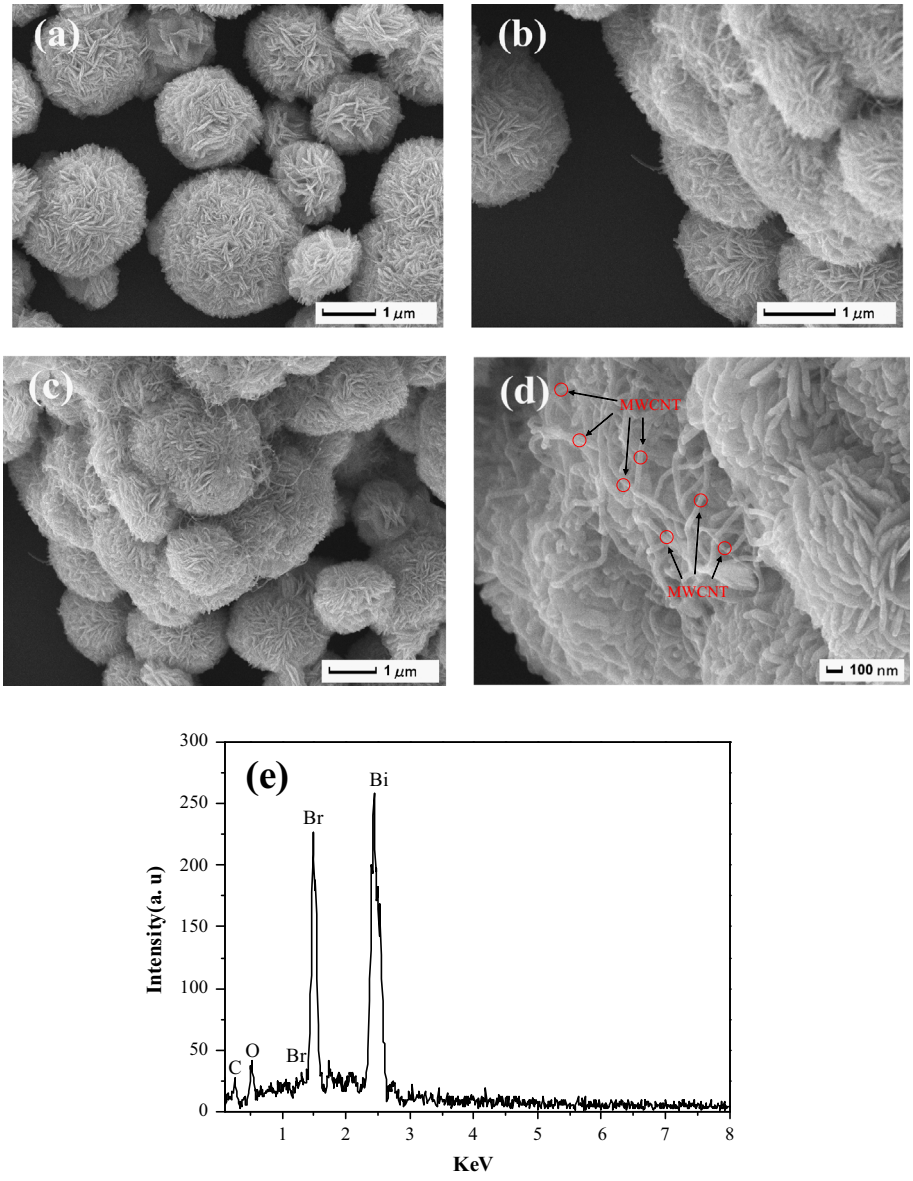

Fig. 4. SEM images of the 0.05 wt% MWCNT/BiOBr microspheres structures. (a) and (b) the low magnification SEM image; (c) top view SEM image; (d) the high magnification SEM image; and (e) EDS of the 0.05 wt% MWCNT/BiOBr microspheres.

composites showed better photocatalytic activity in the visible light. When the MWCNT content was higher than 0.05 wt%, a further increase of MWCNT content caused a decrease in the photocatalytic activity of RhB degradation. It can be speculated that the origin of enhanced photocatalytic activity was attributed to the fact that increased dark color of photocatalysts could absorb more light, leading to generate more electron–hole pairs. Subsequently, MWCNT accelerated the transfer of electrons between the BiOBr interfaces, elevated the separation efficiency of electrons and holes, leading to a higher photocatalytic activity. As we know, MWCNT dispersed on the surface of BiOBr. When the MWCNT content was higher than 0.05 wt%, too many MWCNT would hinder the BiOBr absorb visible light, leading to the decrease of generation of electron–hole pairs.

3.10. The proposed mechanism

The type of radicals in the photocatalytic process played a crucial role for understanding the mechanism during the process of photocatalytic degradation of pollutants. The active ingredient in the photocatalytic process could be detected by trapping experiments of radicals and holes. Tert-butanol and EDTA–2Na were selected as the radicals and holes trapping agent respectively[50]. As shown in Fig. 11, the photodegradation of RhB was obviously depressed after 1mmol EDTA–2Na was added. On the contrary, the photocatalytic activity was slightly suppressed after the injection of 1 mmol Tert-butanol. Therefore, it could be indicated that hole was the main reactive specie for the degradation of RhB.

Based on the results of structure characterizations and the visible light photocatalytic tests of the as-prepared samples, a

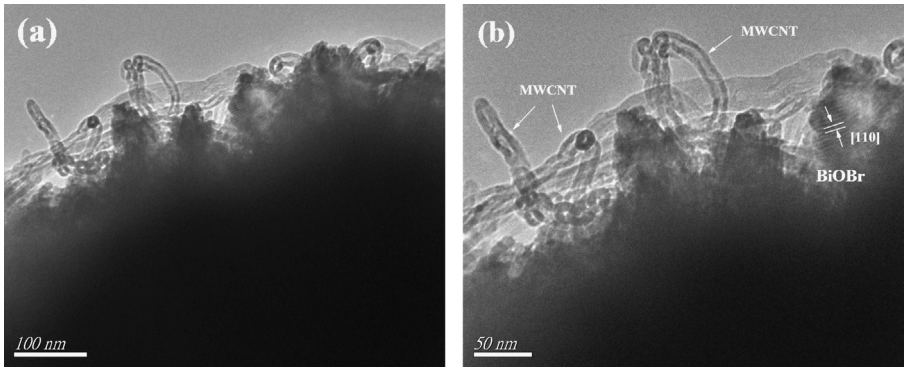

Fig. 5. (a) TEM image of the 0.05 wt% MWCNT/BiOBr composites; (c) HRTEM image of 0.05 wt% MWCNT/BiOBr composites.

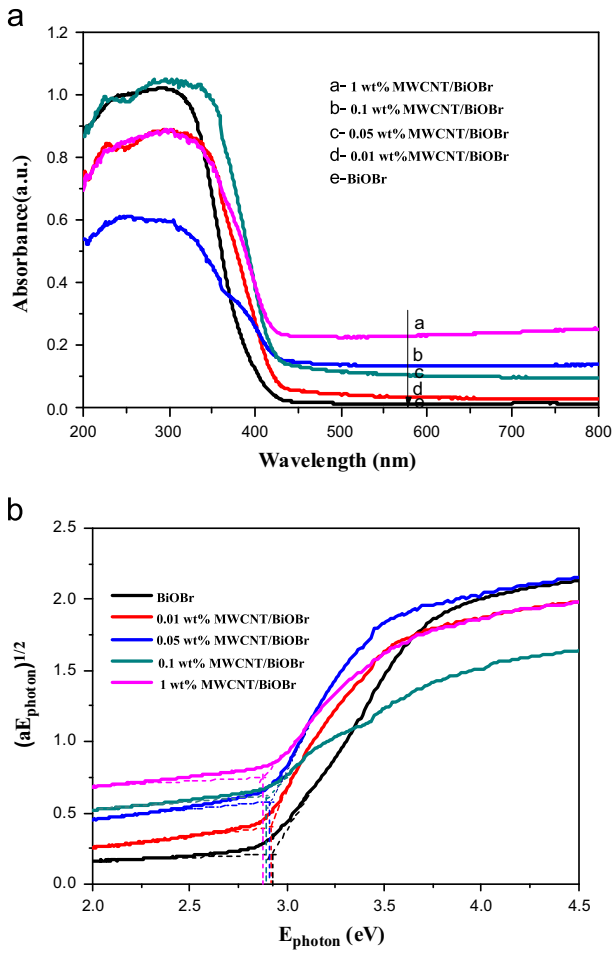

Fig. 6. (a) UV–vis diffuse reflectance spectra of the as-prepared samples and (b) $(\alpha E_{photon})^{1/2}$ vs E_{photon} curves of the as-prepared samples.

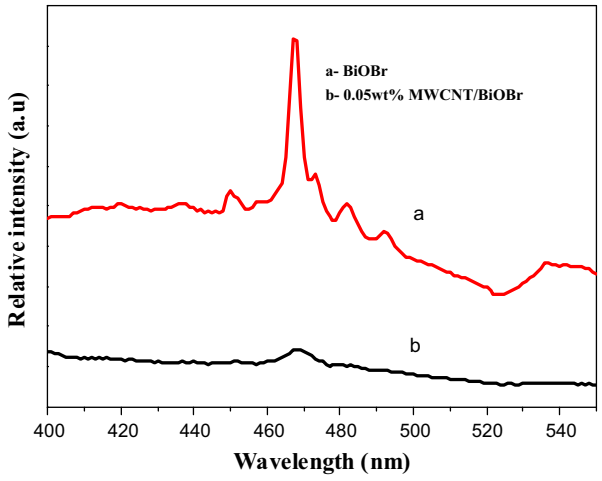

Fig. 7. PL spectra of BiOBr and 0.05 wt% MWCNT/BiOBr materials.

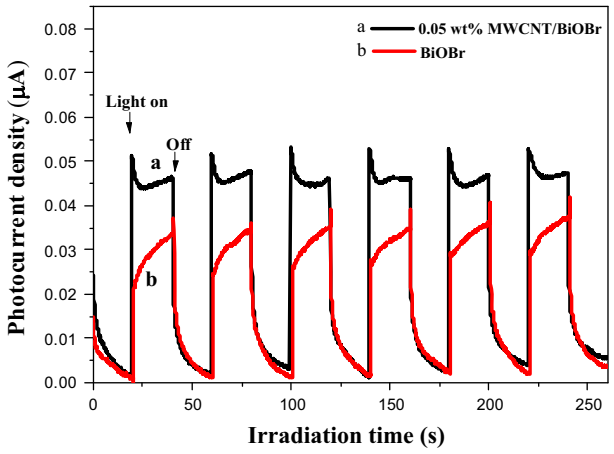

Fig. 8. Transient photocurrent response for the pure BiOBr and 0.05 wt% MWCNT/BiOBr.

possible mechanism of MWCNT on the improvement of visible light performance was proposed and illustrated in Fig. 12. The significant enhancement of photocatalytic performance can be attributed to synergistic effect between BiOBr and MWCNT. When the MWCNT were introduced, the MWCNT dispersed well on the surface of BiOBr microspheres and combined with BiOBr closely on its surface. The MWCNT could act as effective electron transfer channel because they had high electrical conductivity and high electron storage ability [25,28]. As can be seen from Fig. 10, when the system was irradiated by visible light, the BiOBr in the composite photocatalyst was excited and generated electron–hole pairs. The photogenerated electrons in the conduction band (CB) of BiOBr tended to migrate towards the MWCNT, while the holes remained in valance band (VB). The electrons would accumulate on the surface of MWCNT which leads to

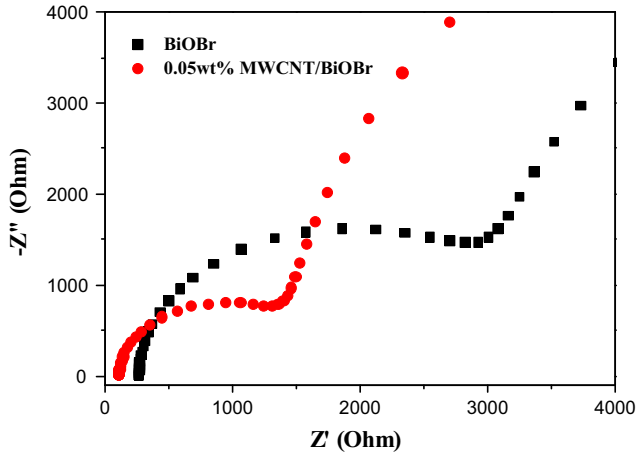

Fig. 9. Electrochemical impedance spectroscopy of BiOBr and 0.05 wt% MWCNT/BiOBr.

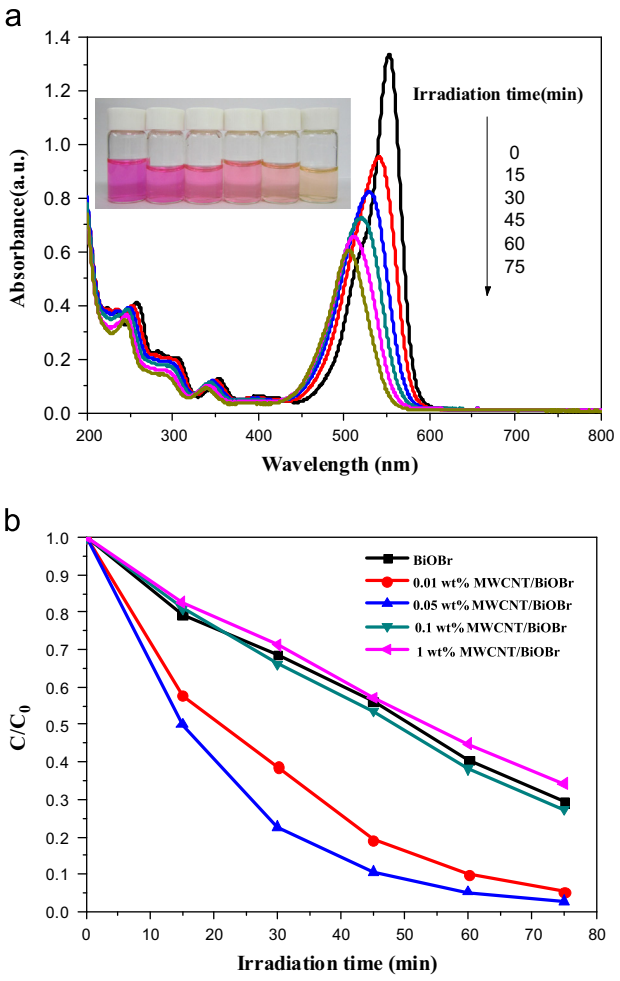

Fig. 10. (a) Effects of MWCNT/BiOBr with different MWCNT contents on RhB degradation efficiency (b) Temporal UV–vis absorption spectral changes during the photocatalytic degradation of RhB in aqueous solution in the presence of 0.05 wt% MWCNT/BiOBr.

efficient separation of electron–hole pairs and effectively reduction of the recombination of photogenerated electrons and holes. The hole at the VB was the main reactive specie for

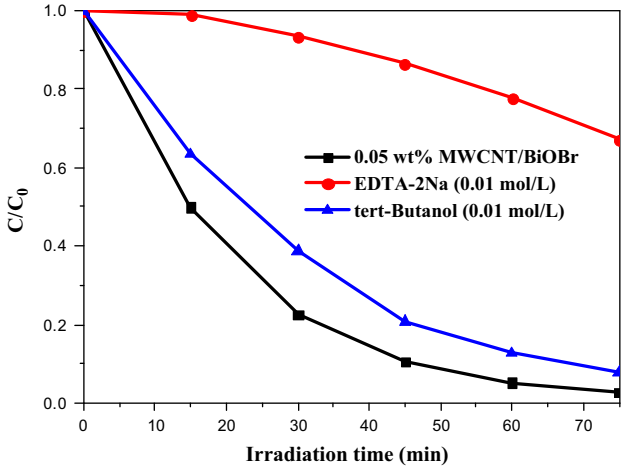

Fig. 11. Comparison of photocatalytic activities of 0.05 wt% MWCNT/BiOBr catalyst for the degradation of RhB with or without adding EDTA–2Na and t-Butanol under visible light irradiation.

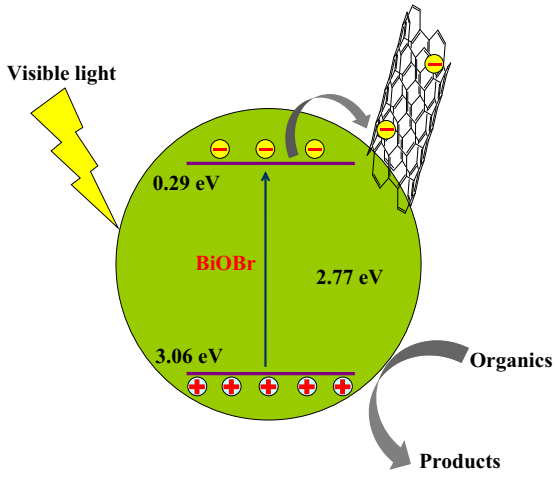

Fig. 12. Schematic of the separation and transfer of photogenerated charges in the MWCNT/BiOBr combined with the possible reaction mechanism of photocatalytic procedure.

the degradation of RhB. Therefore, the MWCNT/BiOBr composite had an enhanced photocatalytic activity.

4. Conclusions

In summary, novel MWCNT/BiOBr composite photocatalysts were successfully prepared in the presence of reactable ionic liquid [C_{16}mim]Br. The structure, morphology and photocatalytic activity have been investigated. SEM analysis indicated that MWCNT/BiOBr composites were flower-like microspheres consisted of numerous nanosheets. It can be clearly found that a large number of MWCNT attached to the surface of BiOBr microspheres. DRS analysis indicated that the bandgaps of MWCNT/BiOBr composites decreased and the absorption intensity of visible light strengthened with the increasing of MWCNT content. An enhanced photocatalytic activity of MWCNT/BiOBr composite photocatalysts has been observed, compared to pure BiOBr. Besides, the addition

amount of the MWCNT had a significant influence on the photoactivity of MWCNT/BiOBr and the optimal MWCNT content was determined to be 0.05 wt%. PL, EIS, and photocurrent analysis of the pholocatalyst, indicated that MWCNT well combined with BiOBr and well dispersed on the surface of BiOBr microspheres facilitated electron–hole separation, which may leading to an enhanced visible light photocatalytic activity. The result of trapping experiments of radicals and holes suggested that holes were the main oxidative species in this system. On the basis of above analysis, the efficient synthesis method in the presence of reactable ionic liquid for MWCNT/BiOBr could be a new method to design new photocatalysts with high performance for environmental applications.

Acknowledgment

This work was financially supported by the National Nature Science Foundation of China (No. 21206060, 21007021 and 21177050), China Postdoctoral Science Foundation (2012 M510125), Jiangsu Province (1102118C), and the Special Financial Grant from the China Postdoctoral Science Foundation (2013T60506).

References

[1] Z.H. Ai, W.K. Ho, S.C. Lee, L.Z. Zhang, Efficient photocatalytic removal of NO in indoor air with hierarchical bismuth oxybromide nanoplate microspheres under visible light, Environmental Science and Technology 43 (2009) 4143.

[2] S.Y. Chai, Y.J. Kim, M.H. Jung, A.K. Chakraborty, D. Jung, W.I. Lee, Heterojunctioned BiOCl/Bi_2O_3, a new visible light photocatalyst, Journal of Catalysis 262 (2009) 144.

[3] S.M. Sun, W.Z. Wang, L. Zhang, L. Zhou, W.Z. Yin, M. Shang, Visible light-induced efficient contaminant removal by Bi_5O_7I, Environmental Science and Technology 43 (2009) 2005.

[4] J. Henle, P. Simon, A. Frenzel, S. Scholz, S. Kaskel, Nanosized BiOX (X=Cl, Br, I) particles synthesized in reverse microemulsions, Chemistry of Materials 19 (2007) 366.

[5] J.X. Xia, S. Yin, H.M. Li, H. Xu, Y.S. Yan, Q. Zhang, Self-assembly and enhanced photocatalytic properties of BiOI hollow microspheres via a reactable ionic liquid, Langmuir 27 (2011) 1200.

[6] J. Lee, Q.W. Zhang, F. Saito, Mechanochemical synthesis of LaOX (X=Cl, Br) and their solid state solutions, Journal of Solid State Chemistry 160 (2001) 469.

[7] N. Kijima, K. Matano, M. Saito, T. Oikawa, T. Konishi, H. Yasuda, T. Sato, Y. Yoshimura, Oxidative catalytic cracking of *n*-butane to lower alkenes over layered BiOCl catalyst, Applied Catalysis A 206 (2001) 237.

[8] J.X. Xia, S. Yin, H.M. Li, H. Xu, L. Xu, Y.G. Xu, Improved visible light photocatalytic activity of sphere-like BiOBr hollow and porous structures synthesized via a reactable ionic liquid, Dalton Transactions 40 (2011) 5249.

[9] W.D. Wang, F.Q. Huang, X.P. Lin, xBiOI–$(1-x)$BiOCl as efficient visible-light-driven photocatalysts, Scripta Materialia 56 (2007) 669.

[10] Z. Jiang, F. Yang, G. Yang, L. Kong, M.O. Jones, T. Xiao, P.P. Edwards, The hydrothermal synthesis of BiOBr flakes for visible-light-responsive photocatalytic degradation of methyl orange, Journal of Photochemistry and Photobiology A – Chemistry 212 (2010) 8.

[11] J. Zhang, F.J. Shi, J. Lin, D.F. Chen, J.M. Gao, Z.X. Huang, X.X. Ding, C.C. Tang, Self-assembled 3-D architectures of BiOBr as a visible light-driven photocatalyst, Chemistry of Materials 20 (2008) 2937.

[12] J.W. Wang, Y.D. Li, Synthesis of single-crystalline nanobelts of ternary bismuth oxide bromide with different compositions, Chemical Communications 18 (2003) 2320.

[13] M. Shang, W.Z. Wang, L. Zhang, Preparation of BiOBr lamellar structure with high photocatalytic activity by CTAB as Br source and template, Journal of Hazardous Materials 167 (2009) 803.

[14] X. Zhang, Z.H. Ai, F.L. Jia, L.Z. Zhang, Generalized one-pot synthesis, characterization, and photocatalytic activity of hierarchical BiOX (X=Cl, Br, I) nanoplate microspheres, Journal of Physical Chemistry C 112 (2008) 747.

[15] J. Fu, Y.L. Tian, B.B. Chang, F.N. Xi, X.P. Dong, BiOBr–carbon nitride heterojunctions: synthesis, enhanced activity and photocatalytic mechanism, Journal of Materials Chemistry 22 (2012) 21159.

[16] X.M. Zhang, X.F. Chang, M.A. Gondal, B. Zhang, Y.S. Liu, G.B. Ji, Synthesis and photocatalytic activity of graphene/BiOBr composites under visible light, Applied Surface Science 258 (2012) 7826.

[17] S. Shenawi-Khalil, V. Uvarov, S. Fronton, I. Popov, Y. Sasson, A. Novel, Heterojunction BiOBr/bismuth oxyhydrate photocatalyst with highly enhanced visible light photocatalytic properties, Journal of Physical Chemistry C 116 (2012) 11004.

[18] J. Cao, B.Y. Xu, B.D. Luo, H.L. Lin, S.F. Chen, Novel BiOI/BiOBr heterojunction photocatalysts with enhanced visible lightphotocatalytic properties, Catalysis Communications 13 (2011) 63.

[19] H. Gnayem, Y. Sasson, Hierarchical nanostructured 3D flowerlike $BiOCl_xBr_{1-x}$ semiconductors with exceptional visible light photocatalytic activity, ACS Catalysis 3 (2013) 186.

[20] L. Kong, Z. Jiang, T.C. Xiao, L.F. Lu, M.O. Jones, P.P. Edwards, Exceptional visible-light-driven photocatalytic activity over BiOBr–$ZnFe_2O_4$ heterojunctions, Chemical Communications 47 (2011) 5512.

[21] H.F. Cheng, B.B. Huang, P. Wang, Z.Y. Wang, Z.Z. Lou, J.P. Wang, X. Y. Qin, X.Y. Zhang, Y. Dai, In situ ion exchange synthesis of the novel Ag/AgBr/BiOBr hybrid with highly efficient decontamination of pollutants, Chemical Communications 47 (2011) 7054.

[22] L.F. Lu, L. Kong, Z. Jiang, H.H.C. Lai, T.C. Xiao, P.P. Edwards, Visible-light-driven photodegradation of rhodamine B on Ag-modified BiOBr, Catalysis Letters 142 (2012) 771.

[23] Z.S. Liu, B.T. Wu, Y.B. Zhu, D.G. Yin, L.G. Wang, Fe-Ions modified BiOBr Mesoporous microspheres with excellent photocatalytic property, Catalysis Letters 142 (2012) 1489.

[24] K. Woan, G. Pyrgiotakis, W. Sigmund, Photocatalytic carbon-nanotube–TiO_2 composites, Advanced Materials 21 (2009) 2233.

[25] A. Kongkanand, P.V. Kamat, Electron storage in single wall carbon nanotubes: Fermi level equilibration in semiconductor-SWCNT suspensions, ACS Nano 1 (2007) 13.

[26] O. Akhavan, M. Abdolahad, Y. Abdi, S. Mohajerzadeh, Synthesis of titania/carbon nanotube heterojunction arrays for photoinactivation of *E. coli* in visible light irradiation, Carbon 47 (2009) 3280.

[27] K.E. Tettey, M.Q. Yee, D. Lee, Photocatalytic and conductive MWCNT/TiO_2 nanocomposite thin films, ACS Applied Materials and Interfaces 2 (2010) 2646.

[28] K. Dai, T.Y. Peng, D.N. Ke, B.Q. Wei, Photocatalytic hydrogen generation using a nanocomposite of multi-walled carbon nanotubes and TiO_2 nanoparticles under visible light irradiation, Nanotechnology 20 (2009) 125603.

[29] Y.Q. Sun, C. Liu, Y.X. Xu, H. Bai, Z.Y. Yao, G.Q. Shi, Chemically converted graphene as substrate for immobilizing and enhancing the activity of a polymeric catalyst, Chemical Communications 46 (2010) 4740.

[30] M.H. Su, C. He, L.F. Zhu, Z.J. Sun, C. Shan, Q. Zhang, D. Shu, R. L. Qiu, Y. Xiong, Enhanced adsorption and photocatalytic activity of BiOI-MWCNT composites towards organic pollutants in aqueous solution, Journal of Hazardous Materials 229 (2012) 72.

[31] L. Ge, C.C. Han, Synthesis of MWNTs/g-C_3N_4 composite photocatalysts with efficient visible light photocatalytic hydrogen evolution activity, Applied Catalysis B 117 (2012) 268.

[32] T.Y. Peng, P. Zeng, D.N. Ke, X.J. Liu, X.H. Zhang, Hydrothermal preparation of multiwalled carbon nanotubes (MWCNTs)/CdS nanocomposite and its efficient photocatalytic hydrogen production under visible light irradiation, Energy and Fuel 25 (2011) 2203.

[33] H.Q. Wu, Q.Y. Wang, Y.Z. Yao, C. Qian, X.J. Zhang, X.W. Wei, Microwave-assisted synthesis and photocatalytic properties of carbon nanotube/zinc sulfide heterostructures, Journal of Physical Chemistry C 112 (2008) 16779.
[34] Z.H. Li, Z.M. Liu, J.L. Zhang, B.X. Han, J.M. Du, Y.N. Gao, T. Jiang, Synthesis of single-crystal gold nanosheets of large size in ionic liquids, Journal of Physical Chemistry B 109 (2005) 14445.
[35] X. Xu, Y. Li, Y.T. Gong, P.F. Zhang, H.R. Li, Y. Wang, Synthesis of palladium nanoparticles supported on mesoporous N-doped carbon and their catalytic ability for biofuel upgrade, Journal of the American Chemical Society 134 (2012) 16987.
[36] K.L. Ding, Z.J. Miao, Z.M. Liu, Z.F. Zhang, B.X. Han, G.M. An, S. D. Miao, Y. Xie, Facile synthesis of high quality TiO_2 nanocrystals in ionic liquid via a microwave-assisted process, Journal of the American Chemical Society 129 (2007) 6362.
[37] L. Ge, X.Y. Jing, J. Wang, S.B. Jamil, Q. Liu, D.L. Song, J. Wang, Y. Xie, P.P. Yang, M.L. Zhang, Ionic liquid-assisted synthesis of CuS Nest like hollow spheres assembled by microlakes using an oil water interface route, Crystal Growth and Design 10 (2010) 1688.
[38] E. Kowsari, G. Faraghi, Synthesis by an ionic liquid-assisted method and optical properties of nanoflower Y_2O_3, Materials Research Bulletin 45 (2010) 939.
[39] Y. Jiang, Y.J. Zhu, Microwave-assisted synthesis of sulfide M_2S_3 (M=Bi, Sb) nanorods using an ionic liquid, Journal of Physical Chemistry B 109 (2005) 4361.
[40] A. Taubert, CuCl nanoplatelets from an ionic liquid-crystal precursor, Angewandte Chemie International Edition 43 (2004) 5380.
[41] L. Wang, L.X. Chang, B. Zhao, Z.Y. Yuan, G.S. Shao, W.J. Zheng, Systematic Investigation on morphologies, forming mechanism, photocatalytic and photoluminescent properties of ZnO nanostructures constructed in ionic liquids, Inorganic Chemistry 47 (2008) 1443.
[42] Y. Sun, W.J. Zheng, Ultrathin $SmVO_4$ nanosheets: ionic liquid-assisted hydrothermal synthesis, characterization, formation mechanism and optical property, Dalton Transactions 39 (2010) 7098.
[43] T. Fukushima, T. Aida, Ionic liquids for soft functional materials with carbon nanotubes, Chemistry—A European Journal 13 (2007) 5048.
[44] J.L. Bideau, L. Viau, A. Vioux, Ionogels, ionic liquid based hybrid materials, Chemical Society Reviews 40 (2011) 907.
[45] S.B. Zhu, T.G. Xu, H.B. Fu, J.C. Zhao, Y.F. Zhu, Synergetic effect of Bi_2WO_6 photocatalyst with C_{60} and enhanced photoactivity under visible irradiation, Environmental Science and Technology 41 (2007) 6234.
[46] X.J. Bai, L. Wang, Y.F. Zhu, Visible Photocatalytic Activity Enhancement of $ZnWO_4$ by Graphene Hybridization, ACS Catalysis 2 (2012) 2769.
[47] D.S. Da, A.K. Alves, C.P. Bergmann, Photocatalytic degradation of methyl orange dye in water solutions in the presence of MWCNT/TiO_2 composites, Materials Research Bulletin 48 (2013) 1845.
[48] I. Shakir, J.H. Choi, M. Shahid, Z. Ali, D.J. Kang, MoO_3–MWCNT nanocomposite photocatalyst with control of light-harvesting under visible light and natural sunlight irradiation, Journal of Materials Chemistry 22 (2012) 20549.
[49] M. Samadi, H.A. Shivaee, M. Zanetti, A. Pourjavadi, A. Moshfegh, Visible light photocatalytic activity of novel MWCNT-doped ZnO electrospun nanofibers, Journal of Molecular Catalysis A: Chemical 359 (2012) 42.
[50] Y.J. Wang, R. Shi, J. Lin, Y.F. Zhu, Enhancement of photocurrent and photocatalytic activity of ZnO hybridized with graphite-like C_3N_4, Energy and Environmental Science 4 (2011) 2922.